Brain Imaging Analysis

F. DuBois Bowman

Department of Biostatistics, Mailman School of Public Health, Columbia University, New York, NY 10032; email: fb2403@columbia.edu

Annu. Rev. Stat. Appl. 2014. 1:61–85

The *Annual Review of Statistics and Its Application* is online at statistics.annualreviews.org

This article's doi:
10.1146/annurev-statistics-022513-115611

Keywords

neuroimaging, fMRI, DTI, connectivity, prediction, activation

Abstract

The increasing availability of brain imaging technologies has led to intense neuroscientific inquiry into the human brain. Studies often investigate brain function related to emotion, cognition, language, memory, and responses to numerous other external stimuli, as well as resting-state brain function. Brain imaging studies also attempt to determine the functional or structural basis for psychiatric or neurological disorders and to examine the responses of these disorders to treatment. Neuroimaging is a highly interdisciplinary field, and statistics plays a critical role in establishing rigorous methods to extract information and to quantify evidence for formal inferences. Neuroimaging data present numerous challenges for statistical analysis, including the vast amounts of data collected from each individual and the complex temporal and spatial dependencies present in the data. I briefly provide background on various types of neuroimaging data and analysis objectives that are commonly targeted in the field. I also present a survey of existing methods aimed at these objectives and identify particular areas offering opportunities for future statistical contribution.

1. INTRODUCTION

Neuroimaging utilizes powerful noninvasive techniques to capture properties of the human brain in vivo. Imaging studies reveal insights about normal brain function and structure, neural processing and neuroanatomic manifestations of psychiatric and neurological disorders, and neural processing alterations associated with treatment response. Several imaging modalities are widely used, including magnetic resonance imaging (MRI), functional MRI (fMRI), diffusion tensor imaging (DTI), positron emission tomography (PET), electroencephalography (EEG), and magnetoencephalography (MEG), among others. These modalities leverage different physiological characteristics to reflect properties of either brain structure or function. This review largely focuses on fMRI, which captures correlates of neural activity, but some of the ideas presented incorporate or extend to other modalities.

1.1. Imaging Modalities

fMRI quantifies brain activity by measuring correlates of blood flow and metabolism. A fundamental concept behind fMRI is that in-vivo neural activity is associated with localized changes in metabolism. As a brain area becomes more active, for example, to perform a memory task, there is an associated localized increase in oxygen consumption. To meet this additional demand, oxygen-rich blood flow to the active brain area increases. Thus, activated brain areas show a relative increase in oxyhemoglobin and a relative decrease in deoxyhemoglobin because the increased supply of oxygen outpaces the increased demand for it.

The most common form of fMRI works by leveraging the magnetic susceptibility properties of hemoglobin in capillary red blood cells. Hemoglobin, which delivers oxygen to neurons, is diamagnetic when oxygenated and paramagnetic when deoxygenated. The MR scanner records blood oxygenation level–dependent (BOLD) signals that vary according to the degree of oxygenation. Thus, fMRI can be used to produce distributed maps of localized brain activity (see **Figure 1*a***). Notably, although I use the phrase brain activity, the BOLD signal measured in fMRI is several steps removed from the actual neuronal activity. MRI works in a conceptually similar manner, except that the MR signal varies according to tissue type, enabling the production of structural

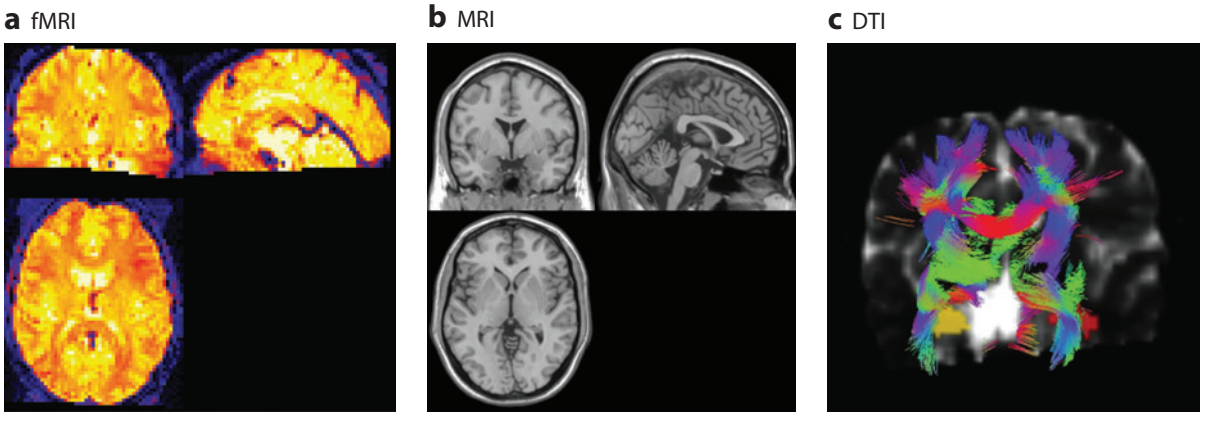

Figure 1

Images of (*a*) distributed patterns of brain activity based on a blood oxygenation level–dependent (BOLD) fMRI scan; (*b*) an anatomical scan revealing gray matter, white matter, and cerebral spinal fluid; and (*c*) probable white-matter tracts based on a tractography algorithm. Abbreviations: DTI, diffusion tensor imaging; fMRI, functional magnetic resonance imaging; MRI, magnetic resonance imaging.

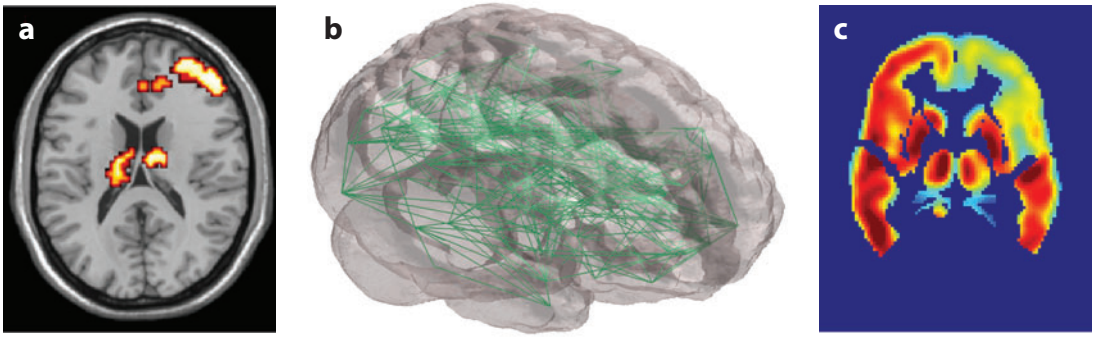

Figure 2

Images displaying results from (*a*) a localization study highlighting brain regions exhibiting increased neural activity from a baseline measure to a posttreatment scanning session for cocaine addicts relative to control subjects, (*b*) a complex network analysis reflecting whole-brain functional connectivity (Simpson et al. 2011), and (*c*) a model yielding predicted maps of postbaseline neural activity, shown here as predicted regional glucose uptake for an Alzheimer's disease patient six months post baseline (Derado et al. 2012).

(i.e., anatomical) images that distinguish gray matter, white matter, and cerebral spinal fluid (see **Figure 1*b***).

DTI is an MRI technique that provides information regarding the structure of white matter in the brain. Neurons are the basic unit of the brain, and humans amazingly have approximately 86 billion neurons (Herculano-Houzel 2012); longstanding estimates are as high as 100 billion neurons (Soc. Neurosci. 2012). Axons are neuron fibers that serve as lines of transmission in the nervous system, and they form (millions of) bundles of textured fibers in the white matter. This extensive system of white-matter bundles directly links some brain structures; association bundles join cortical areas within the same hemisphere, commissural bundles link cortical areas in separate hemispheres, and projection fibers connect areas in the cerebral cortex to subcortical structures (Hendelman 2005). DTI noninvasively maps these white-matter fiber tracts in the brain by measuring the diffusion of water molecules. This technique reveals the presence, integrity, and direction of white-matter fibers because water molecules are more likely to diffuse in the direction of these fibers than perpendicular to them. Further, white-matter fiber tracking techniques portray axonal fibers and structural brain connectivity (see **Figure 1*c***) (Behrens et al. 2003, 2007). Recent National Institutes of Health (NIH) (2009) initiatives such as the Human Connectome Project provide evidence of widespread interest in mapping the structural and functional connectivity of the human brain.

1.2. Common Analysis Objectives

Neuroimaging studies seek insights about normal brain function and structure, neural manifestations of mental and neurological disorders, and neural plasticity associated with treatment response. Associated statistical analyses often center on objectives that target localization, brain connectivity, and prediction or classification. Localization is predicated on the theory of functional specialization—that is, the notion that different areas in the brain are specialized for different functions. Thus, in properly designed studies, one can perform statistical analyses to identify localized changes in the brain that correspond to changes in tasks performed in the scanner. These analyses produce images highlighting statistically significant (or highly probable) task-related changes in neural activity, as illustrated in **Figure 2*a***. Localization studies, also referred to as activation (or neuroactivation) studies, can be extended to identify localized

differences in brain function between groups of subjects (e.g., between schizophrenia patients and healthy controls) and/or between scanning sessions (e.g., differences reflecting treatment-related alterations). To illustrate, **Figure 2*a*** highlights brain regions, such as the middle frontal gyrus and left and right thalamus, that exhibit high probabilities of increased inhibitory control–related neural activity from a baseline measure to a posttreatment period for cocaine addicts relative to corresponding activity changes in control subjects.

Functional connectivity studies seek to identify multiple brain areas that exhibit similar temporal activity profiles, either task-related or at rest. These studies may determine links between a selected seed brain region and all other regions (nodes) considered, dissociate particular brain networks, or generate complex whole-brain networks (see **Figure 2*b***). Researchers may compare functional connectivity properties among subgroups of subjects and between different scanning sessions. Whereas functional connectivity analysis merely targets associations between brain activity in distinct regions, effective connectivity analysis seeks to establish a stronger relationship that reflects the influence that one brain region exerts on another.

Prediction or classification analyses stand to have a significant translational impact. For example, one can use baseline imaging and clinical data to generate maps forecasting metabolic activity in the brain of an Alzheimer's disease patient at a six-month follow-up visit (see **Figure 2*c***). Another example involves the use of imaging and other clinical or biological data to blindly classify individuals into one or more groups, for instance, as either a treatment responder or nonresponder. Such models would have important clinical applications such as aiding in treatment decisions, predicting disease progression, and being used as diagnostic tools when costs are not prohibitive.

Numerous statistical tools have been developed to address these common objectives in brain imaging studies. This review is not intended to offer a complete description of existing approaches in the field; rather, it provides the reader with an overview of select methods for addressing central substantive issues, highlights the analytic challenges that statisticians face in applying existing methods and in developing new ones, and discusses important areas for future research that will benefit from statistical thinking. I begin by describing the data collected in fMRI studies and highlighting attributes of these data that are important for statistical modeling.

2. DATA DESCRIPTIONS, ANALYTIC CHALLENGES, AND PREPROCESSING

fMRI yields dynamic three-dimensional (3D) maps giving second-to-second depictions of distributed brain activity patterns. Studies commonly acquire scans every two to three seconds and may yield hundreds of scans in a single session, but the acquisition speed and duration vary according to study objectives. At the time of statistical analysis, each scan is often arranged in a $91 \times 109 \times 91$ array in which each volume element (or voxel) contains a localized measure of neural activity. **Figure 2*c*** displays a 91×109 array for a selected axial slice across the z-dimension. The temporal evolution of brain activity at a single location (voxel), denoted $\mathbf{Y}_i(v)(S \times 1)$, forms a time series, as **Figure 3** illustrates for two distinct locations. Thus, fMRI data may be regarded either as a collection of hundreds of thousands of time series arising from spatially distinct sources or as a movie of dynamic 3D brain maps. Either of these perspectives reveals the massive amount of data produced in an imaging study: Tens of millions of spatiotemporal neural activity measures are obtained for each subject, and billions of measures are obtained across all subjects in many studies. The enormity of the data set poses challenges for statistical modeling and computation.

Incorporating known biological information into statistical models is often beneficial, but the complexity of the brain presents challenges. One challenge stems from the intricate and massive systems of brain networks, which render correlations that do not necessarily decay with increasing

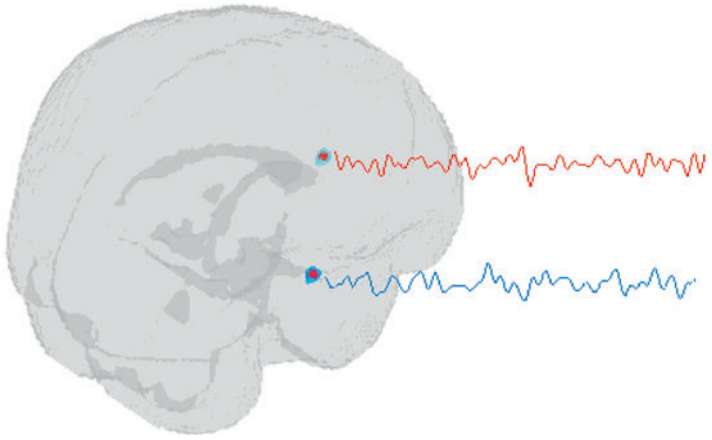

Figure 3

Functional magnetic resonance imaging scans for a single individual may be regarded as tens or hundreds of thousands of time series, two of which are illustrated here. Each time series represents the evolution of measured brain activity at a particular location.

distances. **Figure 4*a*** shows correlations between the fMRI profile for a selected voxel and those from all other voxels in the image. Note that high correlations exist between the selected voxel and many neighboring voxels, voxels at approximately the same location in the opposite hemisphere, and those in some distant areas. These data show obvious departures from an assumption that the strengths of associations decrease with increasing distance (see **Figure 4*b***), thereby posing a major challenge for modeling spatial dependence. Another analytic challenge arising from the ultra-high dimensionality of the data is that many objectives seek to make inferences at each voxel. Thus, one has to cope with multiplicity issues because tens or hundreds of thousands of statistical tests are needed to make such inferences.

Once the data are retrieved from the scanner, they are subjected to a series of processing steps prior to statistical analysis, generally referred to as the preprocessing pipeline. Detailed

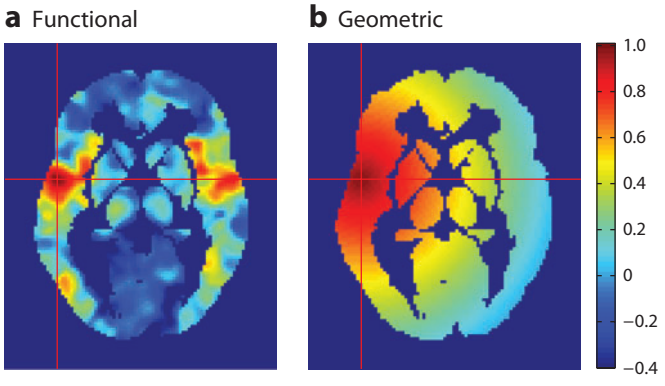

Figure 4

Images displaying (*a*) spatial patterns reflecting correlations between the BOLD signal from a selected voxel (indicated by the cross hairs) and the signals from all other voxels in the image and (*b*) a hypothetical correlation model in which correlations decrease with increasing distance from the selected voxel. The figure reveals that a covariance function specified on the basis of Euclidean distances may be inappropriate for the data.

coverage of preprocessing is beyond the scope of this review, but it is important for the reader to have knowledge of these steps as they may substantially impact subsequent statistical analysis. Our brief remarks omit processing that occurs prior to retrieving data from the scanner. Typical preprocessing steps include (*a*) slice timing correction because each 3D scan representing a single time point actually consists of several 2D slices acquired at slightly different times, (*b*) motion correction to adjust for head movement, (*c*) registration of the fMRI scans to an anatomical MRI scan, (*d*) normalization to warp each individual's set of scans to a standard space for group analysis, (*e*) temporal filtering to address temporal correlations and to remove nonphysiologic trends such as scanner drift, and (*f*) spatial smoothing methods such as convolution with a Gaussian kernel to adjust for residual between-subject neuroanatomic differences that persist following normalization. Spatial smoothing also helps support the assumptions underlying random field theory (discussed in Section 3.2), which is a popular technique to address multiple testing. These preprocessing steps are covered in more detail by Strother (2006), and they are implemented in several neuroimaging software packages, some of which are freely available.

3. SURVEY OF EXISTING METHODS

3.1. Methods for Localization

Localization or activation analyses rely heavily on linear statistical models linking a measure of neural activity to various experimental tasks. The typical strategy uses a so-called mass-univariate approach that fits univariate linear models at each distinct brain voxel (or region) to localize brain areas exhibiting task-related changes. In what follows, I present the basic linear model framework for localization analyses and extensions that fit joint linear models across spatial locations and multiple scanning sessions.

3.1.1. The general linear model. The general linear model (GLM) has been a cornerstone of neuroimaging analyses targeting localization (Friston et al. 1995). A linear mixed model is conceptually well suited for neuroactivation analyses, as it can incorporate subject-specific effects, group-level parameters, and correlations between repeated measures obtained from each individual. The massive amount of data, however, precludes routine use of the mixed model owing to heavy computational demands. As an alternative, a two-stage modeling approach is employed, in which the first stage, a single-subject GLM, is given by

$$\mathbf{Y}_i(v) = \mathbf{X}_{iv}\boldsymbol{\beta}_i(v) + \mathbf{H}_{iv}\boldsymbol{\gamma}_i(v) + \boldsymbol{\varepsilon}_i(v), \qquad 1.$$

where $\mathbf{Y}_i(v)(S \times 1)$ is a vector of S serial brain activity (BOLD) measures for subject i at voxel v, $\mathbf{X}_{iv}(S \times q)$ is the design matrix containing q independent variables, $\boldsymbol{\beta}_i(v)(q \times 1)$ represents the parameter vector linking experimental tasks to the fMRI responses, $\mathbf{H}_{iv}(S \times m)$ contains m additional covariates that are not of substantive interest (e.g., high-pass filtering to remove low-frequency signal drift), and $\boldsymbol{\varepsilon}_i(v)(S \times 1)$ is a vector containing random error about the ith subject's mean (Worsley et al. 2002). I assume $\boldsymbol{\varepsilon}_i(v) \sim \text{Normal}(\mathbf{0}, \boldsymbol{\tau}_v^2\mathbf{V})$, where $\boldsymbol{\tau}_v^2$ is unknown, and $\mathbf{V}$ reflects the correlations between serial BOLD measures.

The BOLD response to neuronal activity is governed by properties of a hemodynamic response function (HRF) (see **Figure 5**). To accommodate the HR properties, researchers generally convolve the design matrix with the HRF using the following equation: $(h * x)(s) = \int_{-\infty}^{\infty} h(\tau)x(s-\tau)\mathrm{d}\tau$. Often, a single HRF model is specified for all voxel locations, but some more flexible methods allow analysts to spatially vary HRFs across voxels (Woolrich et al. 2004a).

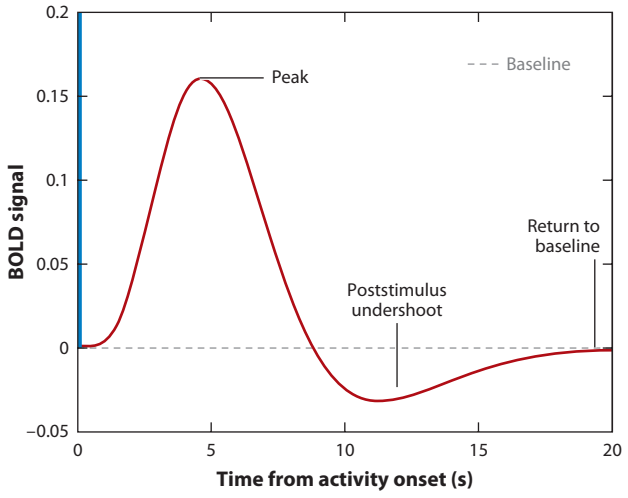

Figure 5

The hemodynamic response function (HRF) following a stimulus-evoked neuronal response. Signal changes include a period of increased blood flow and oxygenation that peaks after roughly five or six seconds, after which the signal falls back toward and temporarily below baseline and is characterized by the poststimulus undershoot.

Next, one models the individualized experimental effects in terms of group-level parameters using a second-stage GLM:

$$\boldsymbol{\beta}_i(v) = \boldsymbol{\mu}(v) + \mathbf{d}_i(v), \qquad 2.$$

where $\boldsymbol{\beta}_i(v)$ contains regression coefficients from Equation 1, $\boldsymbol{\mu}(v)$ is the group-level mean vector, $\mathbf{d}_i(\mathrm{v})$ contains random errors, and $\mathbf{d}_i(\mathrm{v}) \sim$ Normal$(\mathbf{0}, \omega_v^2\mathbf{R})$. One often considers linear contrasts $\mathbf{C}\boldsymbol{\beta}_i(v)$ rather than modeling the entire vector. This two-stage procedure implies the following linear mixed model:

$$\mathbf{Y}_i(v) = \mathbf{X}_{iv}\boldsymbol{\mu}(v) + \mathbf{X}_{iv}\mathbf{d}_i(v) + \mathbf{H}_{iv}\boldsymbol{\gamma}_i(v) + \boldsymbol{\varepsilon}_i(v), \qquad 3.$$

which includes fixed effects given by $\mathbf{X}_{iv}\boldsymbol{\mu}(v)$, random subject-specific effects given by $\mathbf{X}_{iv}\mathbf{d}_i(v)$, and random error introduced by $\boldsymbol{\varepsilon}_i(v)$. The two-stage approach substantially reduces the computational burden because estimation in both GLMs uses least-squares and avoids using either the Newton–Raphson procedure or alternative iterative algorithms required for Equation 3. In practice, one replaces $\boldsymbol{\beta}_i(v)$ in Equation 2 with estimates, say $\hat{\boldsymbol{\beta}}_i(v)$, thereby sacrificing some efficiency relative to fitting the linear mixed model given by Equation 3 directly.

The matrix $\mathbf{V}$, which incorporates covariances between serial BOLD responses, is rarely known in practice, and two strategies are used to estimate the parameters in Equation 1. Prewhitening obtains an initial estimate of the temporal autocorrelation from the data and subsequently transforms $\mathbf{Y}_i(v)$ to remove this correlation (Woolrich et al. 2001). In contrast, precoloring introduces known autocorrelations, say $\mathbf{WY}_i(v)$, through a linear transformation or temporal filtering (Bullmore et al. 1996, Friston et al. 1995, Purdon et al. 2001, Woolrich et al. 2001, Worsley & Friston 1995). The autocorrelations introduced by temporal filtering are deemed to dominate the existing correlations in $\mathbf{V}$. Thus, the resulting covariance structure $\mathrm{Var}(\mathbf{WY}_i(v)) = \tau_v^2\mathbf{WVW}'$ is approximated by $\tau_v^2\mathbf{WW}'$, and estimation proceeds using a weighted least-squares method.

3.1.2. Spatial modeling. Applying the GLM framework to brain imaging data has the apparent limitation that the models are estimated separately for each voxel $v = 1, \ldots, V$; this estimation

method assumes independence between voxels. Several approaches have been developed that incorporate spatial correlations between neural activity from different voxels. The most conceptually straightforward approaches incorporate correlations between a voxel and its contiguous first-order neighbors. Penny et al. (2005) incorporate correlations between in-plane neighboring voxels in a Bayesian model in which the priors for regression parameters rely on a user-specified spatial kernel matrix. Their approach assumes that BOLD responses are spatially homogeneous and locally contiguous within each slice of an image. Katanoda et al. (2002) addressed spatial correlations by including data (for a given voxel) from six physically contiguous voxels in three orthogonal directions. Woolrich et al. (2004b) propose a spatiotemporal Bayesian framework that uses simultaneous autoregressive models for neighboring voxels; this framework allows for both separable and nonseparable models.

As illustrated in **Figure 4**, spatial correlations extend beyond first-order neighbors, may not decrease with increasing distances, and often include long-range associations. Bowman (2007) proposed a linear mixed model (an extended version of Equation 3) that incorporates temporal (repeated measures) correlations using random effects and that captures spatial correlations between voxels by assuming that the strengths of these correlations depend on a measure of the functional distance d_{jk} between the neural activity in voxels j and k (Bowman 2007). Specifically, the model is given by

$$\mathbf{Y}_i = \mathbf{X}_i\boldsymbol{\mu} + \mathbf{Z}_i\boldsymbol{\alpha}_i + \boldsymbol{\epsilon}_i, \qquad 4.$$

where $\mathbf{Y}_i = [\mathbf{Y}_i(1)', \ldots, \mathbf{Y}_i(V)]'$, $\mathbf{Y}_i(v)$ is the same as in Equation 1, and $\mathbf{Z}_i = (\mathbf{I}_V \otimes \mathbf{1}_S)$. The model decomposes the measured BOLD signal into localized mean components $\mathbf{X}_i\boldsymbol{\beta}$, individualized mean-zero random deviations $\boldsymbol{\alpha}_i$ that induce temporal correlations between scans, and random errors that exhibit spatial correlations defined in terms of functional distances (or functional dissimilarities). The model simultaneously incorporates temporal and spatial correlations via $\mathrm{Var}(\mathbf{Y}_i) = (\boldsymbol{\Phi}_i + \mathbf{I}_S) + \sigma_t(\mathbf{I}_V \otimes \mathbf{J}_S)$, where $\mathbf{J}_S$ denotes a unit matrix, and $\boldsymbol{\Phi}_i$ handles parametric covariance structures of the form $(\boldsymbol{\Phi}i)_{jk} = \sigma^2 f(d_{jk})$. Despite its flexibility, this model was proposed for region of interest (ROI) studies, which focus on particular neuroanatomic structures, and intensive computations may limit its applicability to whole-brain studies.

Other methods offer broader spatial coverage for correlations by linking parameters within and between defined brain regions. Bowman (2005) uses a simultaneous autoregressive model to capture exchangeable spatial correlations between all pairs of voxels within functionally defined networks. Using a known parcellation of the brain (see **Figure 6**), Derado et al. (2010) extend this autoregressive model to incorporate repeated measures associations between multiple scanning sessions, such as before and after treatment (Bowman 2005, Derado et al. 2010). Bowman et al. (2008) also leverage the neuroanatomic parcellation to establish a Bayesian framework for incorporating shorter- and longer-range correlations by pooling the jth effect from the model given by Equation 2 across all voxels in brain region g. The second-stage likelihood function for $\boldsymbol{\beta}_{igj} = (\beta_{igj}(1), \ldots, \beta_{igj}(V_g))'$ follows from

$$\boldsymbol{\beta}_{igj} \mid \boldsymbol{\mu}_{gj}, \alpha_{igj}, \sigma^2_{gj} \sim \mathrm{Normal}(\boldsymbol{\mu}_{gj} + \mathbf{1}\alpha_{igj} + \mathbf{X}_i\boldsymbol{\eta}_{gj}, \sigma^2_{gj}\mathbf{I}), \qquad 5.$$

where $\boldsymbol{\mu}_{gj} = (\mu_{gj1}, \ldots, \mu_{gjV_g})'$. Spatial correlations are introduced by modeling the random effects α_{igj} collectively for all G brain regions, $\boldsymbol{\alpha}_{ij} = (\alpha_{i1j}, \ldots, \alpha_{iGj})'$, using the following prior probability distributions:

$$\begin{aligned} \boldsymbol{\alpha}_{ij} \mid \boldsymbol{\Gamma}_j &\sim \mathrm{Normal}(\mathbf{0}, \boldsymbol{\Gamma}_j) \\ \boldsymbol{\Gamma}_j^{-1} &\sim \mathrm{Wishart}\{(h_0\mathbf{H}_{0j})^{-1}, h_0\}. \end{aligned} \qquad 6.$$

Similar to the models proposed by Bowman (2005) and Derado et al. (2010), this model includes exchangeable correlations between voxels within a neuroanatomic region, and $\boldsymbol{\Gamma}_j$ incorporates

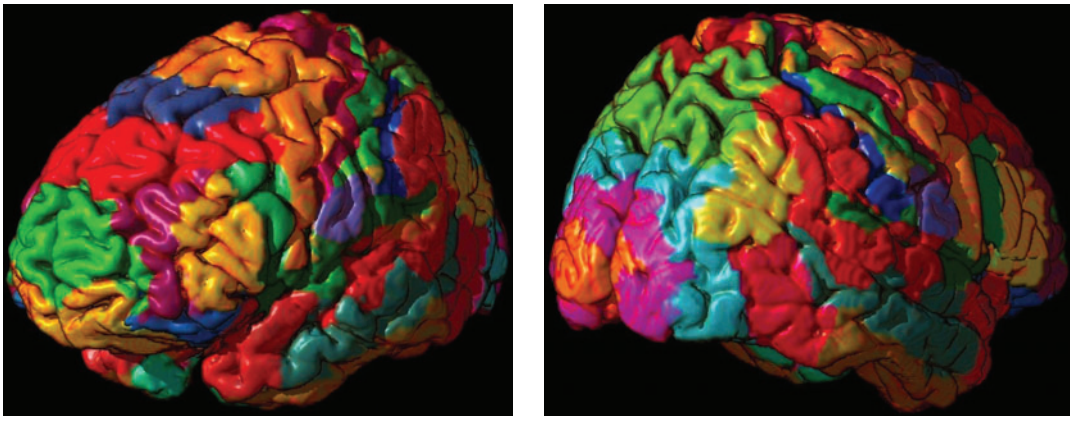

Figure 6

Brodmann areas. Alternative parcellations, such as automatic anatomical labeling, also exist.

between-region correlations. The model provides an excellent compromise between the sophistication needed to address several aspects of spatial and temporal correlations in the data and the simplicity needed to facilitate computational demands, as it can be readily implemented with user-friendly software that makes use of the Gibbs sampler (Zhang et al. 2012). However, this model does not account for dependence between scanning sessions or multiple effects obtained from each individual, and it includes only a relatively simple intraregional correlation model. To overcome these shortcomings, Derado et al. (2012) propose an approach that augments the model given by Equation 5. Their model, which I discuss in Section 3.4, has useful predictive capabilities.

Xu et al. (2009) present an alternative spatial modeling framework that aims to address variability in activation locations across individuals. Collectively, all of the aforementioned spatial modeling extensions offer clear advantages over the standard two-stage GLM, including more suitable modeling assumptions given the properties of the data and underlying neurophysiology, increased precision for estimation, increased statistical power, and expanded interpretations concerning the associations between different brain regions. Spatial smoothing prior to statistical analysis is a standard preprocessing step for fMRI data. The analyst should consider carefully the influence of spatial smoothing, and I recommend either forgoing this procedure during preprocessing or performing very focal spatial smoothing to limit its impact on subsequent spatial modeling and estimation. Despite substantial progress, spatial modeling remains an important area for involvement by statisticians. For example, statisticians may contribute to the development of unified (one-stage) spatiotemporal modeling that integrates supplementary information from other imaging modalities regarding, for example, underlying structural connectivity. Such developments may utilize nonseparable covariance models and multimodal modeling. Note that our use of the term multimodal is consistent with the neuroimaging literature, in which the term describes data from two or more imaging techniques that are combined for analysis, in contrast to the conventional use of the term in statistics to describe distributions with multiple modes.

3.1.3. Unspecified stimulus onset times. Occasionally, studies are designed with unspecified onset times for stimuli that prompt changes in neural activity. For example, if subjects trained in Zen meditation are instructed to focus their awareness by concentrating on breathing while in the scanner, the time at which a subject achieves a deep meditative state may be unknown (Pagnoni et al. 2008). Robinson et al. (2010b) present a model for identifying unknown change points in the data.

Their work estimates the time and duration of evoked changes in neural activity from baseline, and they present a hidden Markov random field model to cluster voxels on the basis of characteristics such as their onset, duration, and anatomical location. Independent component analysis (ICA), which I discuss in Section 3.3, is another approach that does not require a design matrix a priori.

3.1.4. Spectral modeling. Alternatives to modeling fMRI data in the time domain may be based on Fourier or wavelet transformations of the data. Performing such transformations has the primary benefit of simplifying analyses in the transformed space, e.g., because Fourier coefficients are approximately uncorrelated across frequencies and because wavelets have similar decorrelating properties. The approach by Katanoda et al. (2002) discussed above conducts a Fourier domain analysis for their model, which captures spatial correlations between six nearest neighbor voxels. Ombao et al. (2008) present a spatiospectral model that accounts for spatial and temporal correlations using spatially varying temporal spectra to characterize the underlying spatiotemporal processes.

Kang et al. (2012) proposed a spatiospectral mixed-effects model that is conceptually similar to the one in Equations 5 and 6. The linear mixed-effects model is specified for a given frequency band $\boldsymbol{\Omega}_\ell$ as follows:

$$\mathbf{Y}_{gv}(\boldsymbol{\Omega}_\ell) = \mathbf{X}(\boldsymbol{\Omega}_\ell)[\boldsymbol{\mu}_g + \mathbf{b}_{gv}] + \mathbf{d}_g(\boldsymbol{\Omega}_\ell) + \boldsymbol{\varepsilon}_{gv}(\boldsymbol{\Omega}_\ell), \qquad 7.$$

where $g = 1, \ldots, G$ represents the ROIs; $v = 1, \ldots, V_g$ indexes the voxels in ROI g; and $\mathbf{b}_{gv}$, $\mathbf{d}_g(\boldsymbol{\Omega}_\ell)$, and $\boldsymbol{\varepsilon}_{gv}(\boldsymbol{\Omega})_\ell$ are mutually independent and normally distributed. Analysis performed in the frequency domain has associated components for real and imaginary parts, indexed by $j \in \{R, I\}$. Correspondingly, $\mathbf{d}_g(\boldsymbol{\Omega}_\ell) = \mathbf{d}_g^R(\boldsymbol{\Omega}_\ell) + i\mathbf{d}_g^I(\boldsymbol{\Omega}_\ell)$, where $(d_1^j(\boldsymbol{\Omega}_\ell), \ldots, d_G^j(\boldsymbol{\Omega}_\ell))' \sim \text{Normal}(\mathbf{0}, \boldsymbol{\Sigma}_d^j)$; $(b_{g1}^p, \ldots, b_{gV_g}^p)' \sim \text{Normal}(\mathbf{0}, \boldsymbol{\Sigma}_{bg}^p)$ for stimulus p; and $\boldsymbol{\varepsilon}(\boldsymbol{\Omega}_\ell) = \boldsymbol{\varepsilon}^R(\boldsymbol{\Omega}_\ell) + i\boldsymbol{\varepsilon}^I(\boldsymbol{\Omega}_\ell)$, where $\boldsymbol{\varepsilon}^j(\boldsymbol{\Omega}_\ell) \sim \text{Normal}(\mathbf{0}, 0.5\, f(\boldsymbol{\Omega}_\ell)\mathbf{I})$ and $f(\boldsymbol{\Omega}_\ell)$ is the spectrum at frequency band $\boldsymbol{\Omega}_\ell$. The matrix $\boldsymbol{\Sigma}_{bg}^p$ introduces correlations between the V_g voxels within ROI g and assumes that the covariance elements are determined as a function of the Euclidean distances between the corresponding voxels within the ROI. $\boldsymbol{\Sigma}_d^j$ models correlations between the G ROIs, and the simplified covariance structures resulting from the frequency domain model are given by $\text{Var}(\boldsymbol{\varepsilon}^j(\boldsymbol{\Omega}_\ell))$.

Raw fMRI data (usually prior to retrieval from the scanner) are in the Fourier domain, and an inverse Fourier transform converts these data into magnitude, frequency, and phase components. With the raw data, one has the opportunity to model both the magnitude and phase components directly. Rowe (2005) presents a model for complex fMRI data that describes their magnitude and phase and that can be used to test for task-related changes in magnitude, phase, or both. Zhu et al. (2009) also present a Rician regression model that characterizes noise contributions to fMRI data, along with associated estimation and diagnostic procedures.

3.2. Statistical Inferences

Statistical inferences in neuroactivation studies seek to identify localized task-related alterations in brain activity, localized differences in neural activity between groups of subjects, and treatment-related (or other session-related) changes in localized activity. One may target these objectives via a set of null hypotheses $H_0 = \{H_{01}, \ldots, H_{0V}\}$, addressed by linear combinations of group-level effects, e.g., $\mathbf{C}\boldsymbol{\mu}$. For frequentist approaches, one proceeds by calculating an appropriate test statistic, T_v, at each voxel. These statistics are often t- or F-statistics based on the underlying modeling assumptions. One may also consider nonparametric alternatives such as permutation testing for localized inferences (Nichols & Holmes 2002). The goal for any of these approaches, whether frequentist or Bayesian, is to produce activation maps similar to those shown in **Figure 2*a***,

which reveal locations exhibiting significant or highly probable changes (or differences) in neural activity. Given the massive number of tests performed, typically hundreds of thousands, it is desirable to establish some control over the collective testing errors.

For a given search region $\mathcal{R}$, controlling familywise error at a significance level α involves selecting a threshold t_α such that $\Pr[\bigcup_{v=1}^{V}(T_v \geq t_\alpha)\,|\,H_0, \mathcal{R}] \leq \alpha$. Common methods for addressing multiplicity in neuroimaging data include uncorrected approaches that specify an arbitrarily small significance level such as $\alpha = 0.005$, Bonferroni-type procedures, random field theory, permutation testing, and false discovery rate (FDR) approaches. Of these, the Bonferroni, random field theory, and permutation testing methods control familywise error.

The widely used Bonferroni approach selects a threshold t_α such that for each voxel $\Pr[T_v \geq t_\alpha\,|\,H_0, v \in \mathcal{R}] \leq \alpha/V$, which by Boole's inequality ensures that the familywise error is controlled. The number of voxels V is extremely large for whole-brain studies and the test statistics at each voxel are not statistically independent, making the Bonferroni procedure highly conservative. Therefore, this approach rarely yields statistical significance, and in practice, Bonferroni corrections are often adapted to consider the size of an activated cluster.

Random field theory is a mathematically elegant approach that regards a map of localized test statistics as a continuous random field, e.g., a Gaussian, t, F, or χ^2 distributed random field. Any threshold t_α applied to the test statistic map has an associated excursion set containing the voxels for which the localized statistic exceeds the threshold. Random field theory uses a topological property called the Euler characteristic to summarize this set, which Worsley et al. (1992, p. 903) heuristically describe as "the number of isolated parts of the excursion set, irrespective of their shape, minus the number of 'holes'," although the formal definition involves the curvature of the boundary of the excursion set at tangent planes (Adler 1981). As simple examples, the Euler characteristic is 1 for a solid ball and 0 for a doughnut. If no holes are present, then this characteristic counts the number of isolated regions of suprathreshold activation in an image. **Figure 7** illustrates the appearance of isolated regions (blobs) and holes for lower thresholds applied to the t-statistic map (see **Figure 7*a*,*b***), whereas only isolated regions remain for higher activation thresholds (see **Figure 7*c*,*d***). The thresholded maps shown here reflect increases in brain activity associated with increased working memory demands in patients with schizophrenia.

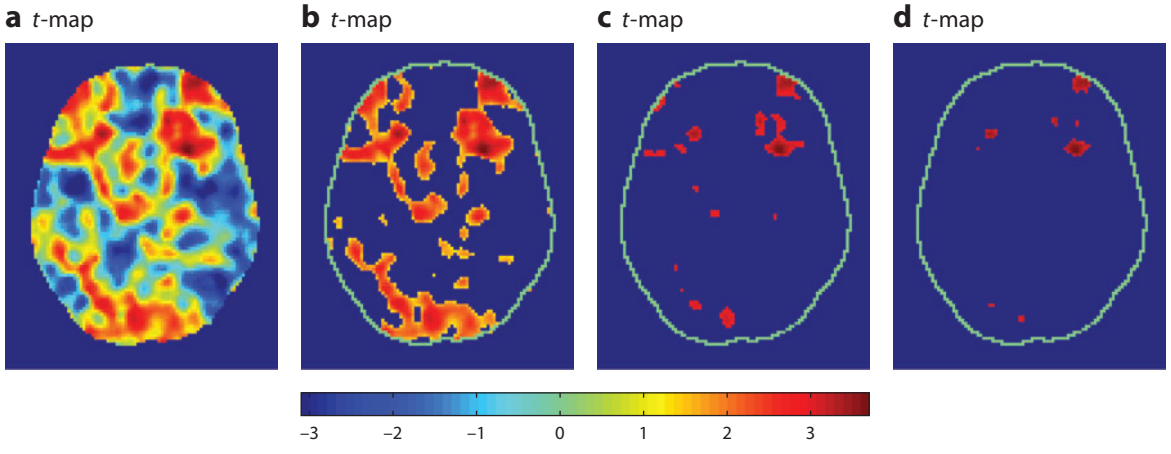

Figure 7

t-Statistic maps with various levels of thresholding. The maps reflect working memory–related differences among individuals with schizophrenia. Features of the Euler characteristic, blobs and holes, appear in panel *b*; only blobs remain as the threshold increases.

Under the null hypothesis for a given search region $\mathcal{R}$, the critical value t_α satisfies $\Pr[T_{\max} > t_\alpha | \mathcal{R}] \leq \alpha$. If t_α is large, then the exceedence probability for the maximum is approximated by the expected value of the Euler characteristic, $\mathrm{E}(\chi_{t_\alpha})$. This probability is given by

$$\begin{aligned} \Pr[T_{\max} > t_\alpha | \mathcal{R}] &\approx \mathrm{E}(\chi_{t_\alpha}) \\ &\approx V |\mathbf{\Lambda}|^{1/2} (2\pi)^{-2} (t_\alpha^2 - 1) e^{-t_\alpha^2/2} \\ &\approx R(4 \log_e 2)^{3/2} (2\pi)^{-2} (t_\alpha^2 - 1) e^{-t_\alpha^2/2}, \end{aligned} \quad 8.$$

where $\mathbf{\Lambda}$ is a matrix of partial derivatives of the random field with respect to the dimensions x, y, and z that can (under a set of assumptions) be approximated as $|\mathbf{\Lambda}|^{1/2} = (\mathrm{FWHM}_x \times \mathrm{FWHM}_y \times \mathrm{FWHM}_z)^{-1} (4 \log_e 2)^{3/2}$ using the full widths at half-maximum (FWHM) of the Gaussian smoothing kernel, and the variable R, given by $R = V/(\mathrm{FWHM}_x \times \mathrm{FWHM}_y \times \mathrm{FWHM}_z)$, is a measure of the number of resolution elements (resels) in the search volume (Worsley et al. 1992).

The random field theory approach is widely used in the neuroimaging community and is easily implemented using available software packages. Criticisms largely target the required assumptions, which are clearly delineated by Nichols & Hayasaka (2003). Considering the Gaussian case, one assumes that under the null hypothesis, the test statistic image can be modeled by a smooth, homogeneous, mean-zero Gaussian random field with unit variance. The level of smoothness should be sufficient to reflect properties of a continuous random field. The random field theory approach works well with extensive levels of smoothing, for example, 10 voxels FWHM, but low smoothness may yield conservative results. The spatial autocorrelation function (ACF) must be twice differentiable at the origin. The random field theory approach assumes that the data are stationary or are stationary after a deformation of space (Worsley et al. 1999). Also, the roughness or smoothness is assumed to be known without appreciable error. Random field theory becomes more conservative with decreasing sample sizes and yields thresholds comparable to those produced by the Bonferroni procedure for data analyses with low degrees of freedom (Nichols & Hayasaka 2003).

Resampling testing procedures, including wavelet-based procedures and traditional permutation testing, have been proposed as alternatives for making statistical inferences about neuroimaging data (Bullmore et al. 2001, 2003, 2004; Nichols & Holmes 2002). Nichols & Holmes (2002) use permutation testing to construct an empirical distribution for the maximum statistic $T_{\max}$. Implementing this technique for fMRI group-level analyses involves permuting labels across individuals that define contrasts or subgroups, computing the voxel test statistics, and determining the $T_{\max}^b$ for each permutation sample $b = 1, \ldots, B$. This computation yields the permutation distribution from the ordered values of the maximum statistic $T_{\max}^{(1)} \leq T_{\max}^{(2)} \leq \cdots \leq T_{\max}^{(B)}$. At significance level α, the critical value is determined from this empirical distribution by the smallest b^* such that $(1 - b^*/B) \leq \alpha$. Once b^* has been identified, any voxel with $T_v > T_{\max}^{(b^*)}$ may be declared statistically significant, and exact p-values may be determined directly from the permutation distribution. Permutation testing has the key advantage that it does not require strong assumptions about the distribution of the data, in contrast to the random field theory approach. Nichols & Holmes (2002) showed that, relative to other testing procedures, permutation tests may yield increases in power with small sample sizes.

FDR has received attention in several large-scale data areas. In contrast to familywise error control, FDR protects against the expected rate of false discoveries (or false positives) among the significant tests (Benjamini & Hochberg 1995, Genovese et al. 2002) and is defined to be 0 when no tests are rejected. FDR offers control according to the following: $\mathrm{E(FDR)} \leq \pi_0 \omega$, where π_0 is the unknown proportion of null hypotheses that are true and ω is the user-specified level of control. In many neuroimaging applications, $\pi_0 \approx 1$ because most voxels will not show any effect.

Thus, although setting $\pi_0 = 1$ is often reasonable, this estimate may be conservative when π_0 is substantially smaller than 1. Adaptive FDR procedures seek less conservative approaches by estimating the unknown quantity π_0. Reiss et al. (2012) reveal vulnerabilities with adaptive FDR, including astonishing paradoxical cases in which adaptive FDR yields more liberal results than not making any correction for multiplicity (Reiss et al. 2012). FDR is easily implemented, for a specified rate ω, by ordering the p-values $p_{(1)} \leq p_{(2)} \leq \cdots \leq p_{(V)}$ for the V voxels and then determining the largest i, say i^*, such that

$$p_{(i^*)} \leq \frac{i^*\omega}{V\left[\sum_{i=1}^{V}(1/i)\right]}. \quad 9.$$

This procedure declares voxels corresponding to $p_{(1)}, \ldots, p_{(i^*)}$ as significant.

FDR is a flexible approach for addressing multiplicity because it is implemented using p-values, which can be produced by a range of models and testing frameworks. FDR does not require smoothed data and, in fact, is more powerful for unsmoothed data. This is a relative strength compared with random field theory, which often requires aggressive smoothing for good performance. Some view FDR as a technique that is best suited to situations in which one seeks to control the number of discoveries that prove to be false at a subsequent validation phase, as for applications targeting preliminary discovery. In neuroimaging, however, activation results from whole-brain analyses tend to be the final goal; neuroimaging studies are not routinely designed with plans to conduct subsequent validation analyses on discovered findings.

3.3. Connectivity

Connectivity analyses stand to reveal insights about the functional interplay between distinct brain regions or between regions in identified networks. Moreover, such analyses may determine the roles that disruptions to these functional associations play in mental and neurological disorders. Below, I describe popular techniques and analytic challenges involved in performing connectivity studies. I present methods for determining undirected associations (functional connectivity) between brain regions as well as stronger directional relationships.

3.3.1. Functional connectivity. Functional connectivity refers to the temporal coherence in neural activity between spatially remote brain regions (Friston et al. 1993) and is examined using various undirected measures of association such as Pearson's correlation coefficient, partial correlation, mutual information, and spectral coherence. Seed-based methods represent one simple approach to determine functional connectivity. These techniques simply identify a set of brain regions, usually via hypothesis-driven selection, and calculate the associations between these seed regions and every other brain region considered, producing correlation images such as that depicted in **Figure 4*a***. To mitigate the impact of varying hemodynamics for different brain regions, one may accommodate time lags between brain regions i and j, e.g., using the following equation:

$$\rho_{ij} = \max_{u \in U}\left\{\frac{\sum_{t=1}^{T-u}[y_i(t+u) - \bar{y}_i][y_j(t) - \bar{y}_j]}{\hat{\sigma}_i\hat{\sigma}_j}\right\}. \quad 10.$$

An area of growing interest for seed-based (and other) connectivity approaches concerns the potential dynamic nature of functional associations or networks, whereby connectivity patterns change dynamically over time. Seed-based procedures remain popular because they are simple to implement and interpret. However, they may miss important findings because they are inherently limited in scope by considering a small number of seed regions. These methods are typically hypothesis driven, but the exact seed locations may heavily influence the findings.

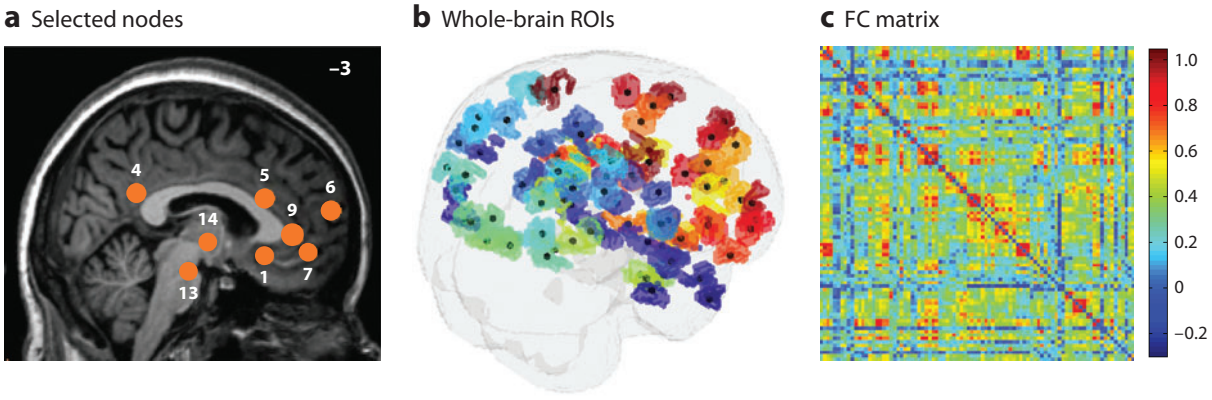

Figure 8

(*a*) Subregions (*orange dots*) thought to be associated with depression, (*b*) subregions representing larger regions from an exhaustive brain parcellation, and (*c*) a matrix of correlations between each pair of regions in panel *b* in which the correlations reflect associations between resting-state brain activity profiles (time series) from pairs of distinct brain regions. Abbreviations: FC, functional connectivity; ROI, region of interest.

Researchers may also determine connectivity by selecting a set of brain regions to serve as nodes and then calculating associations between all nodal pairs. The nodes may target brain regions chosen in a hypothesis-driven manner, such as the putative depression-related regions in **Figure 8*a***, or they may represent subregions drawn from an exhaustive parcellation of the brain; an example is shown in **Figure 8*b***. In either case, associations are computed between every pair of nodes, producing a complete functional connectivity matrix. For example, the connectivity matrix in **Figure 8*c*** corresponds to the 90 whole-brain ROIs shown in **Figure 8*b***: the matrix intensities reflect correlations between the resting-state brain activity profiles from pairs of distinct brain regions. Depending on the objectives, one may scale up to include a larger number of regions to generate whole-brain connectivity networks (see **Figure 2*b***). Ultimately, functional connectivity studies often seek to determine group- or treatment-related differences in connectivity patterns.

Partitioning approaches organize the brain into collections of voxels that have shared properties, for which differences between groupings are larger than those between members of a single group. Two such procedures are independent component analysis (ICA) and cluster analysis. ICA is often motivated by the classic cocktail party problem, in which a researcher seeks to isolate a single voice (or discussion) among those of a group of people who are talking simultaneously in a room. The human brain is quite adept at handling such tasks. Signal processing approaches regard this problem as one of blind source separation, in which the goal is to dissociate a mixture of signals into their originating sources without a priori information about the sources or the mixing process and assuming that the sources are statistically independent.

Letting $\mathbf{Y}(T \times V)$ represent an individual's fMRI data from T scans, ICA decomposes the data into linear combinations of spatiotemporal source signals:

$$\mathbf{Y} = \mathbf{MS} + \mathbf{E}, \qquad 11.$$

where $\mathbf{M}(T \times q)$ is a nonsingular mixing matrix with columns containing latent time series for each of the q independent components, $\mathbf{S}(q \times V)$ is a matrix with rows containing statistically independent spatial signals and columns that are assumed to be non-Gaussian, and $\mathbf{E}(T \times V)$ is a matrix containing noise or variability not explained by the independent components for which each column is assumed to follow a multivariate normal distribution (Beckmann & Smith 2004,

McKeown et al. 1998). Noise-free ICA omits the error term $\mathbf{E}$ (McKeown et al. 1998), implying that $\mathbf{S} = \mathbf{M}^{-1}\mathbf{Y}$ and thereby revealing that $\mathbf{M}^{-1}$ operates as an unmixing matrix that yields statistically independent signals from the fMRI data. Several research groups have developed approaches that extend ICA for group analyses (Beckmann & Smith 2005, Calhoun et al. 2001, Eloyan et al. 2013, Guo 2011, Guo & Pagnoni 2008).

ICA decomposes observed fMRI data into spatially independent sources for which each component has an associated latent time series. Researchers may make putative attributions about the nature of the components; for example, components may be consistently task-related, transiently task-related, or related to other physiologic and nonphysiologic sources. These task-related attributions stem from relating the latent time series to the stimuli, but the interpretation of many components is often challenging and cannot be established with certainty. ICA has a noted advantage relative to modeling approaches such as the GLM in that one can still determine which brain regions are associated with the experimental stimuli without requiring specification of a design matrix. However, ICA does not provide a comprehensive framework for inferences concerning the relationship between the experimental stimuli and the BOLD response. Another advantage of ICA is that noise-related signals revealed by the procedure can be removed from the BOLD response prior to subsequent analyses.

Cluster analysis can also be used to partition the brain into networks of voxels or regions that exhibit similar temporal or task-related dynamics. The statistical literature provides well-established techniques for performing cluster analysis. Several of these data-driven methods have been successfully applied in brain imaging, including the following: K-means approaches (Balslev et al. 2002; Goutte et al. 1999, 2001), fuzzy clustering methods (Baumgartner et al. 2000; Fadili et al. 2000, 2001; Somorjai & Jarmasz 2003), hierarchical clustering methods (Bowman & Patel 2004, Bowman et al. 2004, Cordes et al. 2002, Goutte et al. 2001, Stanberry et al. 2003), a hybrid hierarchical K-means approach (Filzmoser et al. 1999), and dynamical cluster analysis (Baune et al. 1999). Hierarchical clustering generally begins by treating each brain region (or node) as a single cluster, calculating the functional distances between all pairs of brain regions (e.g., $f_{ij} = 1 - \rho_{ij}$, where ρ_{ij} is the partial correlation between regions i and j), and iteratively joining the most similar regions or clusters (recalculating the functional distances at each step). The process ceases when only a single cluster remains. Clustering procedures then examine each stage of the resulting tree to determine the optimal number of clusters, often on the basis of criteria assessing both within- and between-cluster variability. Bowman et al. (2012) present a multimodal approach that combines fMRI with structural connectivity information derived from DTI to determine functional connectivity via cluster analysis. They defined a distance measure

$$d_{ij} = \left(1 - \frac{\pi_{ij}}{\lambda}\right) f_{ij} \qquad 12.$$

for which $\pi_{ij} \in [0, 1)$ is the probability of structural connectivity between brain regions i and j, determined using DTI, and $\lambda \in [1, \infty)$ is an empirically optimized attenuation parameter. This distance incorporates structural connectivity while permitting the clustering of regions (or clusters) on the basis of f_{ij} in the absence of structural connectivity, i.e., when $\pi_{ij} \to 0$. This method generally improves network coherence, particularly in contexts with increased noise in the fMRI signal.

Complex functional brain network analyses have recently emerged in neuroimaging studies. Such methods work in conjunction with approaches that specify a set of brain regions as nodes and then quantify associations between the temporal fMRI profiles for every pair of regions. One may view the resulting map of associations, such as the one shown in **Figure 2*b***, as a system of interacting regions. Network analyses attempt to summarize various characteristics of these whole-brain networks and to then conduct hypothesis tests about their properties. Typical summaries include

graph metrics, such as clustering coefficient, path length, and efficiency, that reflect the network's communication ability (either local or global); centrality metrics such as degree, betweenness, closeness, and eigenvector centrality; and community structure measures, including whole-brain topological properties such as small-worldness (Simpson et al. 2013).

Most methods address undirected networks and thus convey information on whole-brain functional connectivity. Currently, statistical input is needed for proper inference on the basis of network metrics. For example, these metrics are estimated and have associated sampling distributions, but most approaches do not take this variability into account. Comparing brain network properties between groups of subjects also requires statistical thinking for formal inferences.

Simpson et al. (2011) develop a multivariate approach that applies exponential random graph models (ERGMs) to functional brain networks. The approach represents global network structure by locally specified explanatory metrics. Given $i = 1, \ldots, G$ and $j = 1, \ldots, G$, let $\mathbf{W}(G \times G)$ denote a random, symmetric connectivity matrix for which the (i, j)th element $W_{ij} = 1$ if regions i and j pass a minimum connection threshold, resulting in a connecting edge in the graphic representation, and for which $W_{ij} = 0$ otherwise. ERGMs specify

$$\Pr(\mathbf{W} = \mathbf{w}|\mathbf{X}, \boldsymbol{\theta}) = \kappa(\boldsymbol{\theta})^{-1} \exp\{\boldsymbol{\theta}' h(\mathbf{w}, \mathbf{X})\}, \qquad 13.$$

where $h(\mathbf{w}, \mathbf{X})$ is a prespecified network feature, possibly consisting of covariates that are functions of the network (e.g., the number of paths of a specified length) and nodal covariates $\mathbf{X}$ (e.g., the location of a node), $\boldsymbol{\theta}$ is a parameter vector linking the prespecified network feature to the connectivity matrix after accounting for the contributions of other network features in the model, and $\kappa(\boldsymbol{\theta})$ is a normalizing constant. This model yields inferences about whether certain local network properties are observed more than would be expected by chance.

3.3.2. Effective connectivity. Some neuroimaging analyses seek to determine stronger directional relationships than the undirected associations describing functional connectivity. For example, effective connectivity targets the influence that one region exerts on another (Friston et al. 1993). Patel et al. (2006) present an approach that uses a Bayesian model to quantify functional connectivity on the basis of the relative difference between the marginal probability that a voxel, v_1, is active and the probability that v_1 is active conditional on elevated activity in voxel v_2. Larger differences between these conditional and marginal probabilities reflect voxel pairs exhibiting stronger functional connections. This approach also investigates the existence of a stronger hierarchical relationship between each pair of functionally connected voxels using a measure called ascendancy. v_1 is ascendant to v_2 when the marginal activation probability of v_1 is larger than that of v_2. The model yields measures of the degree of functional connectivity between a voxel pair and the degree of ascendancy of one voxel relative to the other.

Structural equation models (SEMs) have been applied to fMRI and PET to determine causal associations between brain regions. SEMs focus on the covariance structure that reflects associations between the variables. Parameter estimation in an SEM minimizes differences between the observed covariances and those implied by a user-defined path (or structural) model. The parameters of the SEM represent the strengths of connections among the brain activity measurements in different regions and correspond to measures of effective connectivity.

Dynamic causal modeling (DCM) regards the brain as a deterministic nonlinear dynamic system that receives inputs and produces outputs, and it uses a Bayesian modeling framework to estimate effective connectivity (Friston 2002, Friston et al. 2003). DCM seeks to estimate parameters at the neuronal level to produce modeled BOLD signals that are maximally similar to the observed BOLD signals. The approach parameterizes effective connectivity in terms of coupling, which represents the influence of one brain region on another (Friston et al. 2003).

Granger causality (GC) has recently gained attention in the neuroimaging literature as a method for establishing directional relationships between the neural activities of two spatially distinct regions. Let $\mathbf{Y}_v = \{Y_v(t), t = 1, \ldots, T\}$ denote a stationary time series reflecting the measured brain activity in voxel v. Consider the model

$$\begin{bmatrix} Y_{v_1}(t) \\ Y_{v_2}(t) \end{bmatrix} = \sum_{j=1}^{p} \mathbf{\Lambda}_j \begin{bmatrix} Y_{v_1}(t-j) \\ Y_{v_2}(t-j) \end{bmatrix} + \begin{bmatrix} \varepsilon_{v_1}(t) \\ \varepsilon_{v_2}(t) \end{bmatrix}, \quad 14.$$

where $\mathbf{\Lambda}_j(2 \times 2)$ is a matrix of unknown coefficients and ε_v represents model error. This model regresses the current value of a time series for one voxel, say v_1, on the histories of v_1 and v_2. Additionally, consider the model

$$Y_{v_1}(t) = \sum_{j=1}^{p} \gamma_j Y_{v_1}(t-j) + e(t), \quad 15.$$

where γ_j is an unknown scalar coefficient relating the current neural activity in voxel v_1 to its own history. Then, GC is defined as

$$C_{v_1 \to v_2} = \ln \left[\frac{\mathrm{Var}(e)}{\mathrm{Var}(\varepsilon_{v_1})} \right], \quad 16.$$

which gives a measure of the extent to which the past values of both v_1 and v_2 help predict the current value of v_1 beyond the extent to which the past values of v_1 alone predict its current value (Granger 1969). Causality is inferred if model fit improves significantly upon including the cross-autoregressive terms.

Critics of GC have raised issues about its practical utility for functional neuroimaging (Friston 2009, Nalatore et al. 2007, Nolte et al. 2008, Tiao & Wei 1976, Wei 1978, Weiss 1984). Their questions center on whether there is sufficient temporal resolution in fMRI data, which often have repetition times of 2 s or more, to ascertain causality from lagged association models. Solo (2011) notes that GC found on a slow timescale, such as that of fMRI data, does not necessarily hold on a faster timescale. He suggests that timescale measurements on the order of milliseconds, such as those of MEG/EEG, are necessary to pursue dynamic causality. This critique is applicable to other effective connectivity approaches based on fMRI data. Also, hemodynamic variations across the brain are likely to swamp any causal lag in the underlying neural time series (Friston 2009, Roebroeck et al. 2005). Measurement noise can reverse the estimated GC direction, and temporal smoothing can induce causal relationships (Smith et al. 2011). Smith et al. (2011) empirically evaluated various directional measures, as well as the performances of several functional connectivity approaches. They observed that although GC and other lagged methods generally perform poorly, the approach proposed by Patel et al. (2006) performs reasonably well.

3.4. Prediction

The recent development of an increasing number of neuroimaging analyses targeting classification and a range of prediction objectives has perhaps the greatest potential for translational impact on functional neuroimaging. Here I consider analysis methods that involve the use of neuroimaging data, possibly coupled with other data, to forecast future neural activity or to predict or blindly classify a clinical outcome or behavioral response. For example, prediction and classification methodology could be used to define imaging markers of depression subtypes, to identify neural patterns of individuals who have a high probability of developing Parkinson's disease among members of an undifferentiated aging population, and to determine distinct neural profiles of patients who respond to a particular therapeutic treatment.

I begin by discussing methods aimed at forecasting future neural activity. Guo et al. (2008) developed a Bayesian model that uses a patient's pretreatment scans and other relevant characteristics to predict the patient's brain activity after a specified treatment regimen. The predicted posttreatment neural activity maps provide objective, clinically relevant information that may be incorporated into the treatment selection process. Let $\mathbf{Y}_{i1}(v)(S_1 \times 1)$ denote the vector of baseline scans for subject i corresponding to voxel v, $\mathbf{Y}_{i2}(v)(S_2 \times 1)$ represent scans from a postbaseline follow-up period, and $\mathbf{Y}_i(v) = (\mathbf{Y}_{i1}(v), \mathbf{Y}_{i2}(v))'$. Guo et al. (2008) fit a GLM for $\mathbf{Y}_i(v)(S \times 1)$ analogous to that specified in Equation 1, but they extended their model by assuming a linear covariance structure for the error term of the second-stage model (analogous to that in Equation 2) to capture the correlations between prebaseline and postbaseline neuroimaging data. Prediction via their proposed method proceeds using the conditional distribution of $[\boldsymbol{\beta}_{i2}(v)|\boldsymbol{\beta}_{i1}, \boldsymbol{\mu}(v)]$. They demonstrated that their prediction framework accurately forecasted posttreatment neural processing in a PET study of working memory in individuals with schizophrenia and in an fMRI study of inhibitory control in cocaine-dependent subjects.

Derado et al. (2012) developed an extended Bayesian spatial hierarchical framework for predicting follow-up neural activity based on an individual's baseline functional neuroimaging data. Their approach increases precision by borrowing strength from the spatial correlations present in the data while handling temporal correlations between different scanning sessions. Let $\boldsymbol{\beta}_{ig}(v) = (\beta_{ig1}(v), \beta_{ig2}(v))'$ represent parameters for both sessions one and two from a first-stage GLM. Extending the models given by Equations 2 and 5, Derado et al. (2012) propose

$$\boldsymbol{\beta}_{ig}(v)|\boldsymbol{\mu}_g, \boldsymbol{\phi}_g, \boldsymbol{\alpha}_{ig}, \boldsymbol{\gamma}_{gv}, \boldsymbol{\Psi}_g \sim \text{Normal}(\boldsymbol{\mu}_g(v) + \boldsymbol{\phi}_g(v) + \boldsymbol{\alpha}_{ig} + \mathbf{X}_{ig}\boldsymbol{\gamma}_g, \boldsymbol{\Psi}_g), \qquad 17.$$

where $\boldsymbol{\phi}_g(v)$ is a spatial dependence parameter for local correlations, $\boldsymbol{\alpha}_{ig}$ is a random effects vector, and $\boldsymbol{\Psi}_g$ is a variance-covariance matrix associated with the repeated scanning sessions. **Figure 9** depicts the framework for temporal and local spatial correlations. Priors addressing spatiotemporal correlations include

$$\begin{aligned}
&\boldsymbol{\phi}(v)|\boldsymbol{\phi}(v'), v \neq v', \boldsymbol{\Sigma}, v = 1 \ldots, V \sim \text{Normal}\left(\rho \sum_{v'} \tfrac{w_{vv'}}{w_{v+}}\boldsymbol{\phi}(v'), \tfrac{1}{w_{v+}}\boldsymbol{\Sigma}\right) \quad (\text{MCAR}(\rho, \boldsymbol{\Sigma})),\\
&\boldsymbol{\Sigma}^{-1} \sim \text{Wishart}((c_2\boldsymbol{\Omega}_2)^{-1}, c_2),\\
&\boldsymbol{\alpha}_i^{(j)}|\boldsymbol{\Gamma}_j \sim \text{Normal}(0, \boldsymbol{\Gamma}_j) \quad (\boldsymbol{\alpha}_i^{(j)} = (\boldsymbol{\alpha}_{i1j}, \ldots, \boldsymbol{\alpha}_{iGj})'),\\
&(\boldsymbol{\Gamma}_j)^{-1} \sim \text{Wishart}\{(b_j H_j)^{-1}, b_j\} \quad j = 1, 2.
\end{aligned} \qquad 18.$$

Hence, their approach addresses spatial correlations between defined neuroanatomical regions via $\boldsymbol{\Gamma}_j$ using an unstructured model, between all voxel pairs within each of the defined brain regions

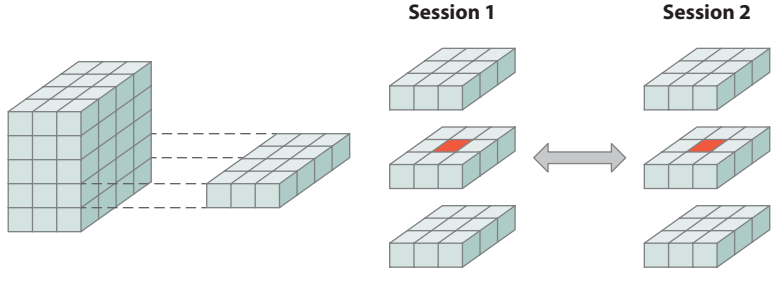

Figure 9

Temporal correlations between repeated measures at a particular voxel location (*red*) and local spatial correlations between 26 third-order neighbors within each scanning session.

using an exchangeable covariance structure, and via a multivariate conditional autoregressive model for the 26 immediate neighbors of each voxel (see **Figure 9**). Correlations due to repeated scanning sessions are captured by the variance-covariance matrix $\mathbf{\Psi}_g$. The method proposed by Derado et al. (2012) demonstrated good performance in a study using PET data to predict disease progression in Alzheimer's disease patients, and their method is also applicable to fMRI data.

Using neuroimaging data to predict a behavioral or clinical response is an increasingly common goal. To make such predictions, one begins with training data $\mathbf{D} = \{\mathbf{X}, \mathbf{y}\}$, where $\mathbf{X}(n \times p)$ is a matrix of p image-derived independent variables (also called features), and $\mathbf{y}$ is a response vector for which $y_i \in \{+1, -1\}$ for binary prediction and $y_i \in \mathbb{R}$ for regression. One then uses the training data to develop a model that yields an accurate prediction of a separate sample $\mathbf{y}^*$ from input variables $\mathbf{x}^*$. I consider the binary case for simplicity, and I include settings in which (*a*) the observation of $\mathbf{y}^*$ follows that of $\mathbf{x}^*$ (prediction) and (*b*) one seeks to blindly distinguish subgroups y_i^* in the absence of an established temporal sequence (classification). Prediction and classification are often based on $\Pr(y_i^* = 1 | \mathbf{x}_i^*, \mathbf{D})$. These studies face challenges resulting from the commonly described curse of dimensionality, which occurs when the number of measures p for each subject (possibly as many as hundreds of thousands) greatly exceeds the number of subjects n (fewer than 50 in many cases).

Support vector machines (SVMs) or support vector classifiers (SVCs) have been one of the most popular tools for prediction or classification in neuroimaging analyses (Casanova et al. 2012, Cox & Savoy 2003, Doehrmann et al. 2013, Dosenbach et al. 2010, LaConte et al. 2005, Mourão-Miranda et al. 2005). In its simplest form, the SVC determines linear boundaries in the feature space, which are used to distinguish between two classes. This framework can be extended to identify nonlinear boundaries and to consider multiclass or regression settings for continuous outcomes. SVM methods do not perform variable selection, but they are able to cope with high-dimensional neuroimaging data structures. The existing literature, coupled with our own experiences applying SVM, suggests that these techniques usually perform well in practice. Chen & Bowman (2011) developed a methodology to apply SVM techniques to longitudinal neuroimaging data; their method uses linear combinations of features from different scanning sessions to make predictions.

Some researchers have proposed related methods for prediction and classification, such as penalized regression, that incorporate a loss function and impose a penalty term on the model complexity. Chu et al. (2011) apply two kernel regression techniques, specifically kernel ridge regression (KRR) and relevance vector regression (RVR). The KRR method implements the dual formulation of ridge regression to facilitate computations, and RVR considers a set of linear basis functions as the kernel and uses sparse Bayesian methods for estimation. Michel et al. (2011a) also present a sparse Bayesian regression approach for multiclass prediction. Their approach initially groups features into several classes and then applies class-specific regularization, thereby attempting to adapt the amount of regularization to the available data. Michel et al. (2011b) apply an ℓ_1 norm of the image gradient, also called the total variation, as regularization. Their method tends to determine block structure, assuming that the neural processing has a sparse spatial layout that is structured in groups of connected voxels. Bunea et al. (2011) apply the widely used Lasso and elastic net procedures to neuroimaging data for prediction and implement a bootstrap-based extension to provide a measure of uncertainty for the variable selection results. Marquand et al. (2010) present a prediction model that uses Gaussian processes to forecast pain intensity from whole-brain fMRI data.

Despite the number of studies pursuing prediction and classification, more principled applications of existing statistical methods are needed, as is the development of new methods. For example, researchers should assess the sensitivity of various approaches to tuning parameters, evaluate the variability involved in assessing generalization accuracy, and incorporate precision

into variable selection techniques. In addition, statisticians have opportunities to apply or develop techniques to leverage the vast and complicated structure present in imaging-derived variables and to incorporate known structure from auxiliary information. Statistics may also play a role in encouraging biological plausibility in the variable selection process.

3.5. Software

Several software packages are available for neuroimaging analysis, many of which are freely accessible and serve as major assets to applied researchers. Some of these packages are fairly comprehensive, implementing various preprocessing steps, statistical analyses, and advanced visualization techniques, but many are specialized for specific analytic methods or data types. I list some popular software tools to aid readers, but I do not attempt to give a complete summary of available packages.

FMRIB Software Library (FSL), developed by the University of Oxford's Center for Functional MRI of the Brain (FMRIB), is a comprehensive library of tools for fMRI, MRI, and DTI. Statistical Parametric Mapping (SPM) is a collection of MATLAB functions equipped with a graphical user interface that offers broad capabilities for preprocessing and analyzing fMRI and MRI data. Similarly, AFNI (often interpreted as an acronym for Analysis of Functional NeuroImages) is a set of C programs for processing, analyzing, and displaying fMRI data. Brain Voyager is a commercial package containing tools for the analysis of fMRI, DTI, EEG, MEG, and transcranial magnetic stimulation (TMS) data. Beyond these comprehensive packages, numerous other software tools can be used to implement specialized analytic methods or to analyze data from a particular modality. Examples of such tools include Bayesian Spatial Model for Activation and Connectivity (BSMac), DTI Studio, Meta-analysis Toolbox, Brain Connectivity Toolbox (BCT), Connectome Workbench, and MedINRIA. As new statistical methods emerge, there remains a need to develop accompanying software that will assist applied researchers in implementing these advanced procedures.

4. DISCUSSION

Neuroimaging is an exciting and rapidly expanding field that is advancing our understanding of the brain and impacting neuroscience, psychology, psychiatry, and neurology. This review provides a survey of major substantive objectives and existing analytic methods, but our summary is by no means comprehensive. Brain imaging research is an inherently interdisciplinary field in which statistics plays a critical role by helping to define rigorous methodology for extracting information and for quantifying statistical evidence.

One area of growing interest is multimodal imaging, which has the potential to incorporate imaging modalities that reflect physiologically distinct, but complementary information. For instance, analysts may combine information extracted from any of the following: brain function, localized properties of tissue density, local diffusion properties, structural connections between regions, and electrophysiological measures of neural activity. These multimodal imaging data may lead to more accurate and reliable analytic approaches than would single-modality analyses, and they also may expand the information content and possible interpretations. Multimodal analyses also provide more complete information by pooling data associated with a physiologically similar objective, such as brain function, measured via blood oxygenation, blood flow, metabolism, and electrical activity. Moreover, various imaging modalities incorporate information across different temporal and spatial scales. Despite the many potential advantages of using multimodal data, these data present challenges for statistical analysis. The dimensionality may become unwieldy. Alignment of information across different temporal scales, say milliseconds to seconds, may cause analytic and interpretative issues. Similarly, integrating information across spatial scales may prove

difficult. Multimodal images may be accompanied by nonimaging data, such as genomic, clinical, demographic, and/or biological information, that exacerbate some of the aforementioned challenges.

A second area for statistical contribution involves the development of methodologies that are able to incorporate biological information. Given the rapid expansion of and intense interest in neuroimaging research, more information will become available to incorporate in future modeling efforts. For example, the NIH-funded Human Connectome Project is an enormous initiative aimed at advancing our knowledge about the human brain and its functional and structural connectivity properties. Also, US President Barack Obama announced the NIH Brain Research through Advancing Innovative Neurotechnologies (BRAIN) Initiative, which is another substantial national investment to aid our understanding of the brain. These and other large-scale initiatives, combined with the rapid expansion of the field more broadly, will provide insights about the brain, offering statisticians an opportunity to develop models that are functionally and structurally better informed. For example, such models may be developed via Bayesian frameworks by incorporating physiologically based prior probability distributions.

Many imaging data sets have nested spatial and temporal structures, which make the Bayesian methodology appealing. Bayesian modeling has proven to be beneficial for neuroimaging data because it distributes the overall complexities of the data across various hierarchical levels and enables flexible posterior inferences. These models, however, often involve many parameters, which may bring about computational issues related to (*a*) Markov chain Monte Carlo methods for posterior simulations and (*b*) assessments of simulation properties such as convergence and the dependence of posterior draws for model parameters. Carefully constructed models, such as those enabling the use of the Gibbs sampler, facilitate computations and are often reasonable to implement in practice. For additional modeling flexibility, however, researchers may need to consider the use of alternative posterior approximation strategies such as variational Bayes to reduce the computational demands.

Some neuroimaging studies are using longitudinal designs instead of traditional cross-sectional designs. The growing number of longitudinal studies and the acquisition of multimodal images raise the issue of missing data. Data for any given subject may be missing from a single measurement occasion or a single modality, making the common practice in neuroimaging studies of discarding all data from subjects who have any missing data an inefficient one. Researchers may make some immediate gains by applying existing methods in the statistical literature for handling missing data to neuroimaging, but the enormity and complexity of imaging data prompt the need for additional methodological development.

fMRI data show substantial variability both within and between subjects, and group studies often have limited sample sizes, prompting the need to consider analytic techniques and study designs that lead to reliable findings. Meta-analyses are one important strategy for determining the degree to which task-related changes in brain activity are consistent across studies and whether pairs or networks of brain regions are consistently simultaneously activated (Cauda et al. 2011, Eickhoff et al. 2009, Kang et al. 2011, Robinson et al. 2010a). Conducting studies with larger sample sizes also yields more precise estimates and more powerful statistical tests, and larger studies including hundreds or even thousands of subjects are beginning to emerge. In summary, neuroimaging is an exciting and rapidly expanding field that presents numerous challenges for quantifying evidence. Statistics should play a critical role in the growth of this interdisciplinary field.

DISCLOSURE STATEMENT

The author is not aware of any affiliations, memberships, funding, or financial holdings that might be perceived as affecting the objectivity of this review.

ACKNOWLEDGMENTS

This article was partially supported by NIH grant U18 NS082143-01.

LITERATURE CITED

Adler RJ. 1981. *The Geometry of Random Fields*. New York: Wiley

Balslev D, Nielsen FA, Frutiger SA, Sidtis JJ, Christiansen TB, et al. 2002. Cluster analysis of activity-time series in motor learning. *Hum. Brain Mapp.* 15(3):135–45

Baumgartner R, Ryner L, Richter W, Summers R, Jarmasz M, Somorjai R. 2000. Comparison of two exploratory data analysis methods for fMRI: fuzzy clustering versus principal component analysis. *Magn. Reson. Imaging* 18(1):89–94

Baune A, Sommer FT, Erb M, Wildgruber D, Kardatzki B, et al. 1999. Dynamical cluster analysis of cortical fMRI activation. *NeuroImage* 9(5):477–89

Beckmann CF, Smith SM. 2004. Probabilistic independent component analysis for functional magnetic resonance imaging. *IEEE Trans. Med. Imaging* 23(2):137–52

Beckmann CF, Smith SM. 2005. Tensorial extensions of independent component analysis for multisubject fMRI analysis. *NeuroImage* 25(1):294–311

Behrens TE, Berg HJ, Jbabdi S, Rushworth MF, Woolrich MW. 2007. Probabilistic diffusion tractography with multiple fibre orientations: What can we gain? *NeuroImage* 34(1):144–55

Behrens TE, Woolrich MW, Jenkinson M, Johansen-Berg H, Nunes RG, et al. 2003. Characterization and propagation of uncertainty in diffusion-weighted MR imaging. *Magn. Reson. Med.* 50(5):1077–88

Benjamini Y, Hochberg Y. 1995. Controlling the false discovery rate: a practical and powerful approach to multiple testing. *J. R. Stat. Soc. B* 57(1):289–300

Bowman FD. 2005. Spatio-temporal modeling of localized brain activity. *Biostatistics* 6(4):558–75

Bowman FD. 2007. Spatiotemporal models for region of interest analyses of functional neuroimaging data. *J. Am. Stat. Assoc.* 102(478):442–53

Bowman FD, Caffo B, Bassett SS, Kilts C. 2008. A Bayesian hierarchical framework for spatial modeling of fMRI data. *NeuroImage* 39(1):146–56

Bowman FD, Patel R. 2004. Identifying spatial relationships in neural processing using a multiple classification approach. *NeuroImage* 23(1):260–68

Bowman FD, Patel R, Lu C. 2004. Methods for detecting functional classifications in neuroimaging data. *Hum. Brain Mapp.* 23(2):109–19

Bowman FD, Zhang L, Derado G, Chen S. 2012. Determining functional connectivity using fMRI data with diffusion-based anatomical weighting. *NeuroImage* 62(3):1769–79

Bullmore E, Brammer M, Williams SC, Rabe-Hesketh S, Janot N, et al. 1996. Statistical methods of estimation and inference for functional MR image analysis. *Magn. Reson. Med.* 35(2):261–77

Bullmore E, Fadili J, Breakspear M, Salvador R, Suckling J, Brammer M. 2003. Wavelets and statistical analysis of functional magnetic resonance images of the human brain. *Stat. Methods Med. Res.* 12(5):375–99

Bullmore E, Fadili J, Maxim V, Sendur L, Whitcher B, et al. 2004. Wavelets and functional magnetic resonance imaging of the human brain. *NeuroImage* 23(Suppl. 1):S234–49

Bullmore E, Long C, Suckling J, Fadili J, Calvert G, et al. 2001. Colored noise and computational inference in neurophysiological (fMRI) time series analysis: resampling methods in time and wavelet domains. *Hum. Brain Mapp.* 12(2):61–78

Bunea F, She Y, Ombao H, Gongvatana A, Devlin K, Cohen R. 2011. Penalized least squares regression methods and applications to neuroimaging. *NeuroImage* 55(4):1519–27

Calhoun VD, Adali T, Pearlson GD, Pekar JJ. 2001. A method for making group inferences from functional MRI data using independent component analysis. *Hum. Brain Mapp.* 14(3):140–51

Casanova R, Hsu FC, Espeland MA, Weiner M, Aisen P, et al. 2012. Classification of structural MRI images in Alzheimer's disease from the perspective of ill-posed problems. *PLoS ONE* 7(10):e44877

Cauda F, Cavanna AE, D'agata F, Sacco K, Duca S, Geminiani GC. 2011. Functional connectivity and coactivation of the nucleus accumbens: a combined functional connectivity and structure-based meta-analysis. *J. Cogn. Neurosci.* 23(10):2864–77

Chen S, Bowman FD. 2011. A novel support vector classifier for longitudinal high-dimensional data and its application to neuroimaging data. *Stat. Anal. Data Min.* 4(6):604–11

Chu C, Ni Y, Tan G, Saunders CJ, Ashburner J. 2011. Kernel regression for fMRI pattern prediction. *NeuroImage* 56(2):662–73

Cordes D, Haughton V, Carew JD, Arfanakis K, Maravilla K. 2002. Hierarchical clustering to measure connectivity in fMRI resting-state data. *Magn. Reson. Imaging* 20(4):305–17

Cox DD, Savoy RL. 2003. Functional magnetic resonance imaging (fMRI) "brain reading": detecting and classifying distributed patterns of fMRI activity in human visual cortex. *NeuroImage* 19(2 Pt. 1):261–70

Derado G, Bowman FD, Kilts CD. 2010. Modeling the spatial and temporal dependence in fMRI data. *Biometrics* 66(3):949–57

Derado G, Bowman FD, Zhang L. 2012. Predicting brain activity using a Bayesian spatial model. *Stat. Methods Med. Res.* 22:382–97

Doehrmann O, Ghosh SS, Polli FE, Reynolds GO, Horn F, et al. 2013. Predicting treatment response in social anxiety disorder from functional magnetic resonance imaging. *JAMA Psychiatry* 70(1):87–97

Dosenbach NU, Nardos B, Cohen AL, Fair DA, Power JD, et al. 2010. Prediction of individual brain maturity using fMRI. *Science* 329(5997):1358–61

Eickhoff SB, Laird AR, Grefkes C, Wang LE, Zilles K, Fox PT. 2009. Coordinate-based activation likelihood estimation meta-analysis of neuroimaging data: a random-effects approach based on empirical estimates of spatial uncertainty. *Hum. Brain Mapp.* 30(9):2907–26

Eloyan A, Crainiceanu CM, Caffo BS. 2013. Likelihood-based population independent component analysis. *Biostatistics* 14(3):514–27

Fadili MJ, Ruan S, Bloyet D, Mazoyer B. 2000. A multistep unsupervised fuzzy clustering analysis of fMRI time series. *Hum. Brain Mapp.* 10(4):160–78

Fadili MJ, Ruan S, Bloyet D, Mazoyer B. 2001. On the number of clusters and the fuzziness index for unsupervised FCA application to BOLD fMRI time series. *Med. Image Anal.* 5(1):55–67

Filzmoser P, Baumgartner R, Moser E. 1999. A hierarchical clustering method for analyzing functional MR images. *Magn. Reson. Imaging* 17(6):817–26

Friston K. 2009. Causal modelling and brain connectivity in functional magnetic resonance imaging. *PLoS Biol.* 7(2):e33

Friston KJ. 2002. Bayesian estimation of dynamical systems: an application to fMRI. *NeuroImage* 16(2):513–30

Friston KJ, Frith CD, Liddle PF, Frackowiak RS. 1993. Functional connectivity: the principal-component analysis of large (PET) data sets. *J. Cereb. Blood Flow Metab.* 13(1):5–14

Friston KJ, Harrison L, Penny W. 2003. Dynamic causal modelling. *NeuroImage* 19(4):1273–302

Friston KJ, Holmes AP, Poline J-B, Grasby PJ, Williams SCR, et al. 1995. Analysis of fMRI time-series revisited. *NeuroImage* 2(1):45–53

Genovese CR, Lazar NA, Nichols T. 2002. Thresholding of statistical maps in functional neuroimaging using the false discovery rate. *NeuroImage* 15(4):870–78

Goutte C, Hansen LK, Liptrot MG, Rostrup E. 2001. Feature-space clustering for fMRI meta-analysis. *Hum. Brain Mapp.* 13(3):165–83

Goutte C, Toft P, Rostrup E, Nielsen F, Hansen LK. 1999. On clustering fMRI time series. *NeuroImage* 9(3):298–310

Granger C. 1969. Investigating causal relations by econometric models and cross-spectral methods. *Econometrica* 37:424–38

Guo Y. 2011. A general probabilistic model for group independent component analysis and its estimation methods. *Biometrics* 67(4):1532–42

Guo Y, Bowman FD, Kilts C. 2008. Predicting the brain response to treatment using a Bayesian hierarchical model with application to a study of schizophrenia. *Hum. Brain Mapp.* 29(9):1092–109

Guo Y, Pagnoni G. 2008. A unified framework for group independent component analysis for multi-subject fMRI data. *NeuroImage* 42(3):1078–93

Hendelman W. 2005. *Atlas of Functional Neuroanatomy*. Boca Raton, FL: CRC. 2nd ed.

Herculano-Houzel S. 2012. The remarkable, yet not extraordinary, human brain as a scaled-up primate brain and its associated cost. *Proc. Natl. Acad. Sci. USA* 109(Suppl. 1):10661–68

Kang H, Ombao H, Linkletter C, Long N, Badre D. 2012. Spatio-spectral mixed effects model for functional magnetic resonance imaging data. *J. Am. Stat. Assoc.* 107(498):568–77

Kang J, Johnson TD, Nichols TE, Wager TD. 2011. Meta analysis of functional neuroimaging data via Bayesian spatial point processes. *J. Am. Stat. Assoc.* 106(493):124–34

Katanoda K, Matsuda Y, Sugishita M. 2002. A spatio-temporal regression model for the analysis of functional MRI data. *NeuroImage* 17(3):1415–28

LaConte S, Strother S, Cherkassky V, Anderson J, Hu X. 2005. Support vector machines for temporal classification of block design fMRI data. *NeuroImage* 26(2):317–29

Marquand A, Howard M, Brammer M, Chu C, Coen S, Mourão-Miranda J. 2010. Quantitative prediction of subjective pain intensity from whole-brain fMRI data using Gaussian processes. *NeuroImage* 49(3):2178–89

McKeown MJ, Makeig S, Brown GG, Jung TP, Kindermann SS, et al. 1998. Analysis of fMRI data by blind separation into independent spatial components. *Hum. Brain Mapp.* 6(3):160–88

Michel V, Eger E, Keribin C, Thirion B. 2011a. Multiclass sparse Bayesian regression for fMRI-based prediction. *Int. J. Biomed. Imaging* 2011:350838

Michel V, Gramfort A, Varoquaux G, Eger E, Thirion B. 2011b. Total variation regularization for fMRI-based prediction of behavior. *IEEE Trans. Med. Imaging* 30(7):1328–40

Mourão-Miranda J, Bokde ALW, Born C, Hampel H, Stetter M. 2005. Classifying brain states and determining the discriminating activation patterns: Support Vector Machine on functional MRI data. *NeuroImage* 28(4):980–95

Nalatore H, Ding M, Rangarajan G. 2007. Mitigating the effects of measurement noise on Granger causality. *Phys. Rev. E* 75(3 Pt. 1):031123

Natl. Inst. Health (NIH). 2009. *The Human Connectome Project.* **http://www.neuroscienceblueprint.nih.gov/connectome**

Nichols T, Hayasaka S. 2003. Controlling the familywise error rate in functional neuroimaging: a comparative review. *Stat. Methods Med. Res.* 12(5):419–46

Nichols TE, Holmes AP. 2002. Nonparametric permutation tests for functional neuroimaging: a primer with examples. *Hum. Brain Mapp.* 15(1):1–25

Nolte G, Ziehe A, Nikulin VV, Schlögl A, Krämer N, et al. 2008. Robustly estimating the flow direction of information in complex physical systems. *Phys. Rev. Lett.* 100:234101

Ombao H, Shao X, Rykhlevskaia E, Fabiani M, Gratton G. 2008. Spatio-spectral analysis of brain signals. *Stat. Sin.* 18:1465–82

Pagnoni G, Cekic M, Guo Y. 2008. "Thinking about not thinking": neural correlates of conceptual processing during Zen meditation. *PLoS ONE* 3(9):e3083

Patel RS, Bowman FD, Rilling JK. 2006. A Bayesian approach to determining connectivity of the human brain. *Hum. Brain Mapp.* 27(3):267–76

Penny WD, Trujillo-Barreto NJ, Friston KJ. 2005. Bayesian fMRI time series analysis with spatial priors. *NeuroImage* 24(2):350–62

Purdon PL, Solo V, Weisskoff RM, Brown EN. 2001. Locally regularized spatiotemporal modeling and model comparison for functional MRI. *NeuroImage* 14(4):912–23

Reiss PT, Schwartzman A, Lu F, Huang L, Proal E. 2012. Paradoxical results of adaptive false discovery rate procedures in neuroimaging studies. *NeuroImage* 63(4):1833–40

Robinson JL, Laird AR, Glahn DC, Lovallo WR, Fox PT. 2010a. Metaanalytic connectivity modeling: delineating the functional connectivity of the human amygdala. *Hum. Brain Mapp.* 31(2):173–84

Robinson LF, Wager TD, Lindquist MA. 2010b. Change point estimation in multi-subject fMRI studies. *NeuroImage* 49(2):1581–92

Roebroeck A, Formisano E, Goebel R. 2005. Mapping directed influence over the brain using Granger causality and fMRI. *NeuroImage* 25(1):230–42

Rowe DB. 2005. Modeling both the magnitude and phase of complex-valued fMRI data. *NeuroImage* 25(4):1310–24

Simpson SL, Bowman FD, Laurienti PJ. 2013. Analyzing complex functional brain networks: fusing statistics and network science to understand the brain. *Stat. Surv.* 7:1–36

Simpson SL, Hayasaka S, Laurienti PJ. 2011. Exponential random graph modeling for complex brain networks. *PLoS ONE* 6(5):e20039

Smith SM, Miller KL, Salimi-Khorshidi G, Webster M, Beckmann CF, et al. 2011. Network modelling methods for FMRI. *NeuroImage* 54(2):875–91

Soc. Neurosci. 2012. *Brain Facts: A Primer on the Brain and Nervous System.* Washington, DC: Soc. Neurosci. **http://www.brainfacts.org/book**

Solo V. 2011. *The dangers of Granger: what they didn't tell you about Granger causality* (*in fMRI*). Presented at Annu. Meet. Org. Hum. Brain Mapp., 17th, June 26–30, Quebec City. **http://www2.warwick.ac.uk/fac/sci/statistics/staff/academic-research/nichols/presentations/ohbm2011/skeptical/Solo_GrangerDanger.pdf**

Somorjai RL, Jarmasz M. 2003. Exploratory analysis of fMRI data by fuzzy clustering—philosophy, strategy, tactics, and implementation. In *Exploratory Analysis and Data Modeling in Functional Neuroimaging*, ed. FT Sommer, A Wichert, pp. 17–42. Cambridge, MA: MIT Press

Stanberry L, Nandy R, Cordes D. 2003. Cluster analysis of fMRI data using dendrogram sharpening. *Hum. Brain Mapp.* 20(4):201–19

Strother SC. 2006. Evaluating fMRI preprocessing pipelines. *IEEE Eng. Med. Biol. Mag.* 25(2):27–41

Tiao G, Wei W. 1976. Effect of temporal aggregation on the dynamic relationship of two time series variables. *Biometrika* 63(3):513–23

Wei WWS. 1978. The effect of temporal aggregation on parameter estimation in distributed lag model. *J. Econom.* 8(2):237–46

Weiss A. 1984. Systematic sampling and temporal aggregation in time series models. *J. Econom.* 26(3):271–81

Woolrich MW, Behrens TE, Smith SM. 2004a. Constrained linear basis sets for HRF modelling using Variational Bayes. *NeuroImage* 21(4):1748–61

Woolrich MW, Jenkinson M, Brady JM, Smith SM. 2004b. Fully Bayesian spatio-temporal modeling of FMRI data. *IEEE Trans. Med. Imaging* 23(2):213–31

Woolrich MW, Ripley BD, Brady M, Smith SM. 2001. Temporal autocorrelation in univariate linear modeling of FMRI data. *NeuroImage* 14(6):1370–86

Worsley KJ, Andermann M, Koulis T, MacDonald D, Evans AC. 1999. Detecting changes in nonisotropic images. *Hum. Brain Mapp.* 8(2–3):98–101

Worsley KJ, Evans AC, Marrett S, Neelin P. 1992. A three-dimensional statistical analysis for CBF activation studies in human brain. *J. Cereb. Blood Flow Metab.* 12(6):900–18

Worsley KJ, Friston KJ. 1995. Analysis of fMRI time-series revisited—again. *NeuroImage* 2(3):173–81

Worsley KJ, Liao CH, Aston J, Petre V, Duncan GH, et al. 2002. A general statistical analysis for fMRI data. *NeuroImage* 15(1):1–15

Xu L, Johnson TD, Nichols TE, Nee DE. 2009. Modeling inter-subject variability in fMRI activation location: a Bayesian hierarchical spatial model. *Biometrics* 65(4):1041–51

Zhang L, Agravat S, Derado G, Chen S, McIntosh BJ, Bowman FD. 2012. BSMac: a MATLAB toolbox implementing a Bayesian spatial model for brain activation and connectivity. *J. Neurosci. Methods* 204(1):133–43

Zhu H, Li Y, Ibrahim JG, Shi X, An H, et al. 2009. Regression models for identifying noise sources in magnetic resonance images. *J. Am. Stat. Assoc.* 104(486):623–37

Annual Review of Statistics and Its Application

Volume 1, 2014

Contents